Preprints (www.preprints.org) | NOT PEER-REVIEWED | Posted: 27 June 2022 doi:10.20944/preprints202206.0352.v1

Article

Zn-Mn Doped Mesoporous Bioactive Glass Nanoparticles Loaded Zein Coatings for Bioactive and Antibacterial Orthopedic Implants

Syeda Ammara Batool [1], Khalil Ahmad [1], Muhammad Irfan [2], Muhammad Atiq Ur Rehman [1,*]

[1] Department of Materials Science and Engineering, Institute of Space Technology Islamabad, Islamabad 44000, Pakistan
[2] School of Chemical and Materials Engineering (SCME), National University of Sciences and Technology (NUST) H-12, Islamabad 44000, Pakistan
* Correspondence: atique1.1@hotmail.com

Abstract: In recent years, natural polymers have replaced synthetic polymers for antibacterial orthopedic applications owing to their excellent biocompatibility and biodegradability. Zein is a biopolymer found in corn. The lacking mechanical stability of zein is overcome by incorporating bioceramics e.g. mesoporous bioactive glass nanoparticles (MBGNs). In present study, pure zein and zein/Zn-Mn MBGNs composite coatings were deposited via electrophoretic deposition (EPD) on 316L stainless steel (SS). Zn and Mn were co-doped in MBGNs in order to make use of their antibacterial and osteogenic potential, respectively. A Taguchi design of experiment (DoE) study was established to evaluate the effect of various working parameters on the morphology of the coatings. It was observed that coatings deposited at 20 V for 5 min with 4 g/L concentration (conc.) of Zn-Mn MBGNs showed highest deposition yield. Uniform coatings with highly dispersed MBGNs were obtained adopting these optimized parameters. Scanning electron microscopy (SEM), energy dispersive spectroscopy (EDS), X-Ray diffraction (XRD), and fourier transform infrared spectroscopy (FTIR) were employed to investigate the morphology and elemental composition of zein/Zn-Mn MBGNs composite coating. Surface properties i.e. coating roughness and wettability analysis concluded that composite coatings were appropriate for cell attachment and proliferation. For adhesion strength various techniques including tape test, bend test, pencil hardness test, and tensile test were performed. Wear and corrosion analysis highlighted the mechanical and chemical stability of coatings. Colony forming unit (CFU) test showed that zein/Zn-Mn MBGNs composite coating was highly effective against *Staphylococcus aureus (S. aureus)* and *Escherichia coli (E. coli)* due to the presence of Zn. The formation of hydroxyapatite (HA) like structure upon immersion in simulated body fluid (SBF) validated the in vitro bioactivity of the coating. It was concluded that zein/Zn-Mn MBGNs coating synthesized in this work can be used for bioactive and antibacterial orthopedic applications.

Keywords: electrophoretic deposition; mesoporous bioactive glass nanoparticles; adhesion; antibacterial; bioactive

1. Introduction

The worldwide market of orthopedic implants is estimated to reach at $66,636 million by the year 2025 due to increased rate of chronic diseases, trauma and age factors [1].

Bio-implants based on metallic and ceramic composite materials provide properties like chemical stability and strength along with good biocompatibility and bioactivity [2]. These features and increased demand urged research in orthopedic implants industry. Metallic implants exhibit relatively low corrosion resistance and uncontrolled leaching of toxic metal in psychological environment. Released metal ions may cause tissue damage caused by carcinogens [3–5].

© 2022 by the author(s). Distributed under a Creative Commons CC BY license.

Preprints (www.preprints.org) | NOT PEER-REVIEWED | Posted: 27 June 2022 doi:10.20944/preprints202206.0352.v1

In this context, present studies are focused on inducing positive response from body organs at the site of implantation [6–8]. The materials selected for substrate and coating should be able to bond with the soft and hard tissues and mimic the structure of natural bone. This requires the materials to be bioactive and form a hydroxyapatite (HA) like structure on the surface of implant [9,10]. The challenges in orthopedic implants are to overcome corrosion and toxic metal ions release while improving bioactivity and resistance towards bacterial attack [11–13].

Zein is a natural biopolymer obtained from the endosperm of maize. It is biocompatible and biodegradable material composed of prolamin [14]. In recent years, owing to the favorable properties, zein is being used as a coating material on implants, targeted drug delivery and tissue engineering applications [15–18]. However, zein has low mechanical strength and for this reason it is usually mixed with inorganic ceramic materials like silicate glasses particularly 45S5 bioactive glass (BG), hydroxyapatite (HA) and calcium phosphates etc. [19–21]. These inorganic materials are bioactive therefore, they promote the bone formation. The brittle nature of ceramics is compensated by the ductility of zein and the deficient mechanical stability of zein is overcome by the ceramics. Hence, the resulting composite performs better in both aspects i.e. in biological as well as mechanical terms [20].

Moreover, it is important to consider the antibacterial effect because the formation of bacterial film over the surface of metallic implants is a major reason for infections [22,23]. To prevent this, the metallic ions (e.g. silver, copper, zinc etc.) are incorporated in biopolymer-ceramic composites. Furthermore, to enhance the osteogenic properties of implants, therapeutic ions such as Mn and Sr are added [24–27].

In general, polymeric materials for biomedical applications are heat sensitive and room temperature processing maintains their natural framework. Electrophoretic deposition (EPD) is a facile, cost-effective and convenient deposition method operating at room temperature [28]. EPD has the advantage of producing uniform coatings over complex shaped orthopedic implants of any size [29]. The suspension for EPD composed of biopolymer, ceramic particles and metallic incorporations is prepared at first step and deposited over substrate of choice in the second step. The working parameters in the EPD process such as voltage, time for deposition, concentration of the suspension, and temperature etc. can be easily altered according to the coating requirements [30] however, it is a time-taking and tedious job to carry out the deposition by considering these factors one-by-one. The adaptation of Taguchi design of experiment (DoE) approach minimizes the number of experiments. The data acquired from the experimental runs is analyzed through software Minitab™ [31]. It provides the optimum working conditions at which suitable coatings can be deposited [32–34].

Kaya et al. [35] deposited zein coatings on stainless steel (SS) substrate for the first time. Homogeneous coatings with high deposition rate were obtained at various voltages and times, proving EPD a suitable method for deposition of zein. In recent years zein was deposited over Ti and Mg substrates other than SS for orthopedic applications [21,30]. However, SS still remains the first choice for the short term implantable devices due to the ease of availability and cost effectiveness. The focus of ongoing research on SS implants is to enhance its biological properties while mitigating the inherent flaws [36,37].

In this work, a composite coating based on zein and mesoporous BG nanoparticles (MBGNs) is prepared for orthopedic applications. The co-deposition of zein and Zn-Mn MBGNs via EPD is being investigated. The mesoporous structure of BG helps in augmented osteoinduction by providing active surface area for osteoblast cells to attach and proliferate. Zn and Mn are added for antibacterial and osteogenic effect, respectively. The doping of metallic ions in MBGNs to produce synergetic antimicrobial effect and osteogenesis is the recent trend [38,39].

To the best of author's knowledge, the coatings comprising of zein and Zn-Mn MBGNs have not been studied before for orthopedic applications. Furthermore, the ap-

Preprints (www.preprints.org) | NOT PEER-REVIEWED | Posted: 27 June 2022 doi:10.20944/preprints202206.0352.v1

plication of Taguchi DoE approach to optimize zein/Zn-Mn MBGNs coating is being studied for the first time. Thus the DoE approach will help in determining the significant factor (i.e. voltage, time, and conc.) affecting the quality of deposits which in turn, help understand the deposition kinetics of zein based composite coatings.

Hence, this study will contribute to the current literature available on antibacterial coatings with enhanced bioactivity and mechanical stability. The aim of this study is to study the suitability of mechanically stable zein/Zn-Mn MBGNs to inhibit biofilm growth and promote bioactivity of the coatings.

2. Materials and methods

2.1. Materials

Zein powder and acetic acid (99.8%) were purchased from Sigma-Aldrich &VWR International, respectively. Zn-Mn doped mesoporous bioactive glass nanoparticles (Zn-Mn doped MBGNs) with nominal composition of SiO_2:70 mol.%, CaO:22 mol.%, Mn:5 mol.% and Zn:3 mol.% were synthesized by modified Stöber process [40]. The precursors such as hexadecyltrimethylammonium bromide (CTAB)-98% (Sigma-Aldrich), zinc nitrate hexahydrate (Sigma-Aldrich), calcium nitrate (Avantar), manganese chloride (Uni-Chem), tetraethyl orthosilicate (TEOS)-99% (Sigma-Aldrich) and ethyl acetate (99.5 %, Merck) were used to prepare MBGNs. The Zn-Mn MBGNs were used in zein suspension for composite coatings on AISI 316L stainless steel (called 316L SS hereafter) substrates. Absolute ethanol (≥ 99.8%, VWR International) and distilled water (ELGADV 25 PURELAB option R7BP) were used to prepare zein/Zn-Mn MBGNs suspension. Acetone (99.5%, Merck) was used to clean 316L SS before depositing composite coatings.

2.2. Suspension Preparation

In order to deposit the composite coating, 316L SS having dimensions of 3cm×1.5cm×0.05cm was used. To prepare suspension for coating, 6 wt.% zein was added to the solution containing 6 vol.% distilled water and 20 vol.% acetic acid in 100 mL of beaker. Later on, 1, 2, 3, and 4 g/L Zn-Mn MBGNs were added in zein mixture to prepare four different types of suspension [19].

This mixture was magnetically stirred (SCI-LOGEX, MS-H280-Pro) for 30 minutes at room temperature to disperse the zein particles homogeneously. Afterwards 74 vol.% of absolute ethanol was added. The suspension was kept in the sonication bath for ~ 30 min in order to ensure the uniform dispersion of Zn-Mn MBGNs in the suspension as reported in [42]. Finally, the suspension was magnetically stirred for 30 min. The pH of suspension was measured by Hanna HI98108 pH meter and maintained at ~3 by adding acetic acid drop wise.

Before coating, 316L SS was ultrasonicated in 50 mL mixture composed of 25 vol.% ethanol, 25 vol.% acetone and 50 vol.% distilled water and dried in air. An area of 2.25 cm^2 was selected to deposit coatings on 316L SS. Figure 1 shows schematic representation of the preparation steps for stable suspension of zein/Zn-Mn MBGNs and subsequent deposition of composite coating on 316L SS.

Preprints (www.preprints.org) | NOT PEER-REVIEWED | Posted: 27 June 2022 doi:10.20944/preprints202206.0352.v1

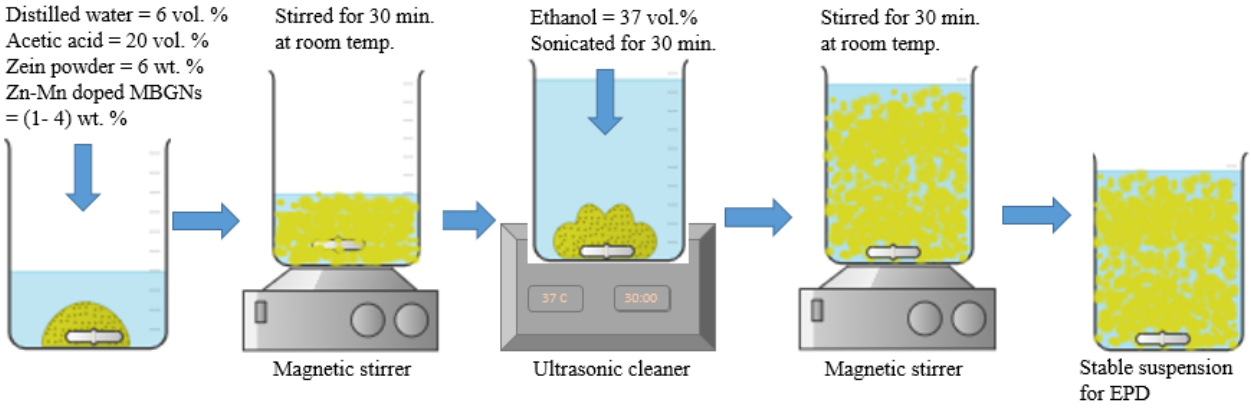

Figure 1. Schematic representation for the preparation steps of zein/Zn-Mn MBGNs stable suspension to deposit composite coating on 316L SS.

Zein/Zn-Mn MBGNs suspensions were prepared with various concentrations of Zn-Mn MBGNs as given in Table 1.

Table 1. Composition of zein/Zn-Mn MBGNs suspensions used to deposit composite coating.

Types of Suspensions	Composition				
	Zn-Mn MBGNs (g/L)	Zein (g/50mL)	Acetic acid (mL/50 mL)	Ethanol (mL/50 mL)	Distilled water (mL/50mL)
1	1	3	3	37	10
2	2	3	3	37	10
3	3	3	3	37	10
4	4	3	3	37	10

The concentration of Zn-Mn MBGNs in the suspension was selected following the study of Pawlik et al. [42]. It was shown that higher the concentration of Zn-Mn MBGNs, poor the suspension stability. On the other hand, the concentration <1 g/L of Zn-Mn MBGNs lead towards poor bioactivity and mitigated antibacterial behavior. Thus, the concentration of 1-4 g/L of Zn-Mn MBGNs was selected in the current study.

2.3. Zeta potential measurement

The zeta potential of pure zein and Zn-Mn MBGNs suspensions was measured in ethanol. The stability of the suspensions was evaluated using zetasizer (Malvern instruments, UK). Three measurements were obtained for each suspension and average value is reported with standard deviation.

2.4. Electrophoretic Deposition

In this work, stable suspension of zein/Zn-Mn MBGNs was prepared and then deposited on 316L SS (cathode) by EPD. The counter electrode (anode) of same material and dimensions was used to complete the circuit. The inter-electrode separation during EPD was maintained at 10 mm. The constant current was applied by DC power supply (eTM-605). Zein showed a positive zeta potential at pH~2.6 and moved towards the cathode upon the application of electric field. It was hypothesized that Zn-Mn MBGNs were encapsulated by the positively charged zein molecules [43].

2.5. Taguchi Design of Experiment (DoE) Approach

In order to optimize the parameters and suspension composition for EPD, a Taguchi array of experiments was designed by using the software (Minitab 17™, Beijing, China)

Preprints (www.preprints.org) | NOT PEER-REVIEWED | Posted: 27 June 2022 doi:10.20944/preprints202206.0352.v1

which gave an array of 16 runs. Three control factors, applied voltage (A), deposition time (B) and conc. of Zn-Mn MBGNs in zein suspension (C) were used to construct an orthogonal Taguchi DoE array. Four levels were assigned to each factor, as illustrated in Table 2.

Table 2. Control factors along with four levels of deposition parameters.

Symbol	Control factors	Levels			
		1	2	3	4
A	Voltage (V)	5	10	15	20
B	Time (min)	1	3	5	7
C	Conc. of Zn-Mn MBGNs (g/L)	1	2	3	4

The control factors were varied according to the selected levels and their effect on deposition yield (mass of zein/Zn-Mn MBGNs composite coating) was taken into consideration.

According to DoE array, 16 experiments were performed as shown in Table 3. Each experiment was repeated three times and average value of deposition yield, standard deviation, and signal to noise ratio (S/N) for deposition yield was calculated.

Table 3. Experimentally measured values of deposition yield and the corresponding standard deviation, S/N ratio for the deposition yield and S/N ratio for standard deviation for EPD of zein/Zn-Mn MBGNs composite coating.

Run	Control factors			Deposition yield in mg/cm²	S/N ratio of deposition yield (dB)	Standard deviation	S/N ratio of standard deviation (dB)
	Voltage (V)	Time (min)	MBGNs Conc. (g/L)				
1	5	1	1	0.17	-15.56	0.001	65.1485
2	5	3	2	0.20	-14.11	0.003	50.6404
3	5	5	3	0.26	-11.77	0.001	61.8456
4	5	7	4	0.27	-11.28	0.008	41.9239
5	10	1	2	0.25	-12.15	0.003	50.8454
6	10	3	1	0.28	-10.97	0.006	44.7428
7	10	5	4	0.96	-0.36	0.005	45.3928
8	10	7	3	1.04	0.34	1.363	-2.6900
9	15	1	3	0.36	-8.94	0.001	58.7529
10	15	3	4	0.90	-0.90	0.016	35.8934
11	15	5	1	0.61	-4.41	0.004	49.0038
12	15	7	2	1.05	0.46	0.095	20.4046
13	20	1	4	0.70	-3.08	0.008	42.4813
14	20	3	3	0.99	-0.12	0.002	52.2514
15	20	5	2	0.92	-0.73	0.008	41.6981
16	20	7	1	0.90	-0.96	0.004	48.5342

Eq.1 was used to calculate the deposition yield.

$$\text{Deposition yield} = \frac{\Delta \text{ weight}}{\text{A in } (\frac{\text{mg}}{\text{cm}^2})} \quad (1)$$

Where Δ weight = weight after coating - weight before coating, while A = area of coating.

Preprints (www.preprints.org) | NOT PEER-REVIEWED | Posted: 27 June 2022 doi:10.20944/preprints202206.0352.v1

It was aimed to obtain higher deposition yield coating with lower value of standard deviation. The S/N ratio for deposition yield was calculated by using Eq. 2 considering that the higher value of deposition yield results in better coatings.

$$\frac{S}{N} \text{ ratio of deposition yield} = -10 \log\left[\frac{1}{n}\left(\sum \frac{1}{y^2}\right)\right] \quad (2)$$

Where y = deposition yield, n = no. of observations

The ratio of S/N for standard deviation was calculated using Eq. 3 by considering that the lower value of standard deviation results in better coatings.

$$\frac{S}{N} \text{ ratio of deposition yield} = -10 \log\left[\frac{1}{n}(\sum y^2)\right] \quad (3)$$

Where y = deposition yield, n = no. of observations

The 48 experiments were performed in total. Each substrate before and after deposition was weighed by using a digital microbalance (Shimadzu-AUY220) (accurate up to 10 mg).

2.6. Characterization of Zein/Zn-Mn MBGNs Composite Coating

2.6.1. Morphological Analysis

The morphological analysis of composite coating was carried out by using high resolution field emission scanning electron microscope (FE-SEM, MIRA, TESCAN). The thickness of pure zein coating and zein/Zn-Mn MBGNs composite coating was also examined. Cross-section of samples were prepared by grinding on sand paper (grit size600) and then cleaned with blower to remove any loosely bound particles on the edges. The qualitative compositional analysis of composite coating was carried out by energy-dispersive X-ray spectroscope (EDX) paired with SEM.

2.6.2. Fourier Transformation Infrared (FTIR) Analysis

Composite coating was also assessed by the attenuated total reflection fourier transformation infrared (ATR-FTIR) spectroscope (Thermofisher-Nicolet Summit Pro) equipped with a quest-ATR unit (diamond crystal). The intensity spectrum was recorded in transmittance mode in the range of 4000-500 cm^{-1}, with Happ-Genzel apodization, at 40 scan per spectrum and the resolution of 4 cm^{-1}. The equipment was integrated with OMNIC paradigm software.

2.6.3. Surface roughness

The average and maximum surface roughness of composite coating was evaluated by Laser profilometer (UBM, ISC-2). A line of 5-7 mm length was drawn on the coated surface to measure the roughness of surface of each sample (scanning velocity of 400 points per second). Bare 316L SS, zein-coated and zein/Zn-Mn MBGNs composite coated samples were subjected to this test for comparison.

2.6.4. Wettability test

Contact angle (CA) was calculated by manually placing a 5 µL droplet of water on the surface of bare 316L SS and composite coated sample with the help of a microliter pipette. The images of the droplet were taken using a digital camera after 5 sec of dropping. The contact angle between surface and drop was measured by analyzing the images in ImageJ™ software.

2.6.5. Adhesion tests

Tape test: Tape test was used to evaluate the qualitative adhesion strength of composite coating deposited by the standard ASTM D3359-17, elaborated in detail in [44]. The results of the tape test were judged with optical microscope (Novex, Holland). Small

Preprints (www.preprints.org) | NOT PEER-REVIEWED | Posted: 27 June 2022 doi:10.20944/preprints202206.0352.v1

squares of 1 mm^2 were marked on the coated surface by applying shear force to the coating. Strong adhesive tape was applied to the coating area and pressed. After 90 seconds, the tape was pulled off from the substrate. The adhesion strength of composite coating was analyzed by the quantity of peeled off coating from the substrate.

Tensile test: The tensile adhesion test was carried out by tensile pull-off method according to ASTM D4541-17 [45] and ISO 4624 [46]. Tensile pull-off test was carried out by applying magic epoxy (made in Pakistan) between two bare surfaces of 316L SS (reference sample). Similarly, epoxy was applied between one coated and one non-coated surfaces. The dimensions of samples (60 mm × 30 mm × 0.5 mm) were same for both sets. After the epoxy dried, both set of samples were subjected to tensile testing (HD-615A-S) by pulling the steel strips upon exerting a force perpendicular to the coated surface in effort to remove these strips. The force was recorded at which the sample strips were detached from each other.

Pencil scratch test: Pencil scratch test according to the ASTM D3363-20 [47] was used for the evaluation of adhesion strength of composite coating. The coated samples were placed on the horizontal solid surface and tested by a set of graded pencils from hard (2H) to soft grade (8B). The sharpened stub of pencil was placed at an angle of 45° against the coated surface. This test was started with the hardness of 2H and continued down the hardness range until the pencil could not scratch the coated surface anymore.

Bend test: Zein/Zn-Mn MBGNs coatings were subjected to a bend test according to ASTM B571-97 [48]. This test determined the deformation ability of composite coatings. The coated samples were bent at 180° with the help of tweezers to examine any kind of detachment, crack or any distortion. The samples of dimension (60 mm × 30 mm × 0.5 mm) were used for this purpose.

Wear test: Wear test was performed on pure zein and composite coatings using Tribometer (MT/60/NI, Spain). Total sliding distance was kept 50 m and 1 N load was applied on the coatings with a 6 mm diameter stainless steel ball indenter at 30 rpm. The wear test was performed under dry conditions at room temperature. All tests for adhesion were done in triplicate and average results are reported.

2.6.6. Corrosion behavior

The corrosion behavior of coating and bare substrate was investigated using potentiodynamic polarization scan. Gamry instrument (reference 600) powered three-electrode system with sample as a working electrode, Ag/AgCl as a reference electrode while graphite as a counter electrode was used. All potentiodynamic polarization scans were recorded at 37 °C in simulated body fluid (SBF) electrolyte at 2.5 mV/s scan rate. The corrosion potential (E_{corr}) and corrosion current density (I_{corr}) were measured directly by extrapolation of Tafel region.

2.6.7. Antibacterial analysis (colony forming unit)

Zein/Zn-Mn MBGNs coated samples were subjected to antibacterial test. Colony forming unit (CFU) method was opted to check the bacterial inhibition potential of the coating. The coated sample (1 cm × 1 cm) was first incubated in the nutrient broth inoculated with *Staphylococcus aureus (S. aureus)* and *Escherichia Coli (E. coli)* separately at 37 °C in a shaking incubator. After 48 hours, the supernatant (at 11000 rpm for 10 min) was collected and further incubated with both bacteria at 37 °C for 24 hours. 50 µL aliquots of both solutions collected after serial dilutions were spread over agar plates and incubated at same conditions. Finally, after 24 hours, number of colonies were counted. The control plates consisted of bacterial cultures without any addition of test samples.

2.6.8. In-vitro bioactivity

To investigate the in vitro bioactivity of coating in terms of hydroxyapatite (HA) formation, the SBF was prepared in laboratory according to the method proposed by Kokubo

Preprints (www.preprints.org) | NOT PEER-REVIEWED | Posted: 27 June 2022 doi:10.20944/preprints202206.0352.v1

et al. [49]. The coated samples of dimensions (10 mm × 10 mm × 0.5 mm) were immersed in 30 mL of SBF and were then incubated at 37 °C for 1, 2, 3, 5, and 7days. The pH was measured after 24 hours for each sample and SBF was changed after every two days to maintain the ionic concentration of the test medium. At each time point, samples were removed from SBF, rinsed with de-ionized water, left to dry in air, and then stored in a desiccator. The weight of samples was measured before and after treating in SBF at each time point. The formation of HA was examined with SEM/EDX. For comparison, samples before immersion in SBF were also characterized.

3. Results and discussion

3.1. Morphology of the synthesized Zn-Mn MBGNs

The Zn-Mn MBGNs were synthesized via modified Stöber process. SEM of synthesized particles was carried out to confirm the morphology and to calculate the average particle size as shown in Figure 2. The inset figure presents the calculated diameter of three different particles (Figure 2A). The average particle size of the as-synthesized Zn-Mn MBGNs was around 90-100 nm. The particles were round shaped, porous and well dispersed. The porous morphology of the particles was due to the Stöber process. In the physiological environment, circular particles have excellent flow properties. However, a little morphological change in the as-synthesized particles does not affect the final properties of the coating [50,51]. The elemental composition of as-synthesized Zn-Mn MBGNs is shown in Figure 2B. Area analysis indicates the presence of Si, Ca, Zn, and Mn, thus confirming the doping of Zn and Mn in MBGNs.

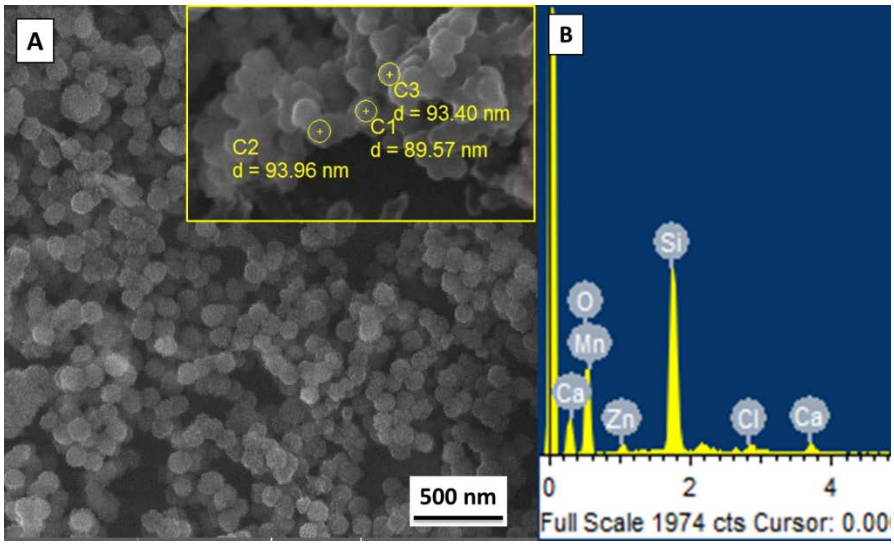

Figure 2. (A) SEM image showing the morphology and size of as-synthesized Zn-Mn MBGNs (B) EDX spectrum confirms the presence of Zn, Mn, Ca, and Si.

3.2. Suspension stability

The suspension stability was appraised measuring zeta potential of the suspensions. The zeta potential of pure zein suspension was + 27.6 ± 11.8 mV and for zein/Zn-Mn MBGNs suspension, it was + 18.3 ± 6.7 mV. The deposition was cathodic owing to the positive zeta potential of the zein molecules. The positive charge on the surface of Zn-Mn MBGNs and subsequent repulsive force (F_R) among Zn-Mn MBGNs and cationic zein molecules contributed towards the sufficient suspension stability.

Zeta potential is a function of pH and electrostatic forces of interaction between suspended particles [52]. For the sufficient electrophoresis of particles, the zeta potential should exhibit a value around + 30 mV. Below this value the particles will become unstable and agglomerate [53]. On the other hand, the very high values of zeta potential also result

Preprints (www.preprints.org) | NOT PEER-REVIEWED | Posted: 27 June 2022 doi:10.20944/preprints202206.0352.v1

in the mitigated electrophoretic mobility. The reason being the electric field may not overcome the forces of repulsion between particles rendering them unable to move in the direction of applied field. The suspension stability is assured by the repulsive electrostatic forces between cationic zein molecules.

Zein molecule is chemically comprised of amine (NH_2) and carboxyl (COOH) groups [35]. It has both hydrophilic as well as hydrophobic domains. Due to the insolubility of zein in water, it is mostly referred as hydrophobic [54]. Although zein is positively charged in the suspension, there remain some functional groups that are negatively charged i.e. COO^-. These charges may interact with oppositely charged molecules and induce electrostatic forces of attraction (F_A) between zein and Zn-Mn MBGNs as illustrated in Figure 3, thus forming a stable suspension. Pishbin et al. [55] also proposed a co-deposition mechanism of chitosan and BG suspension by charge stabilization.

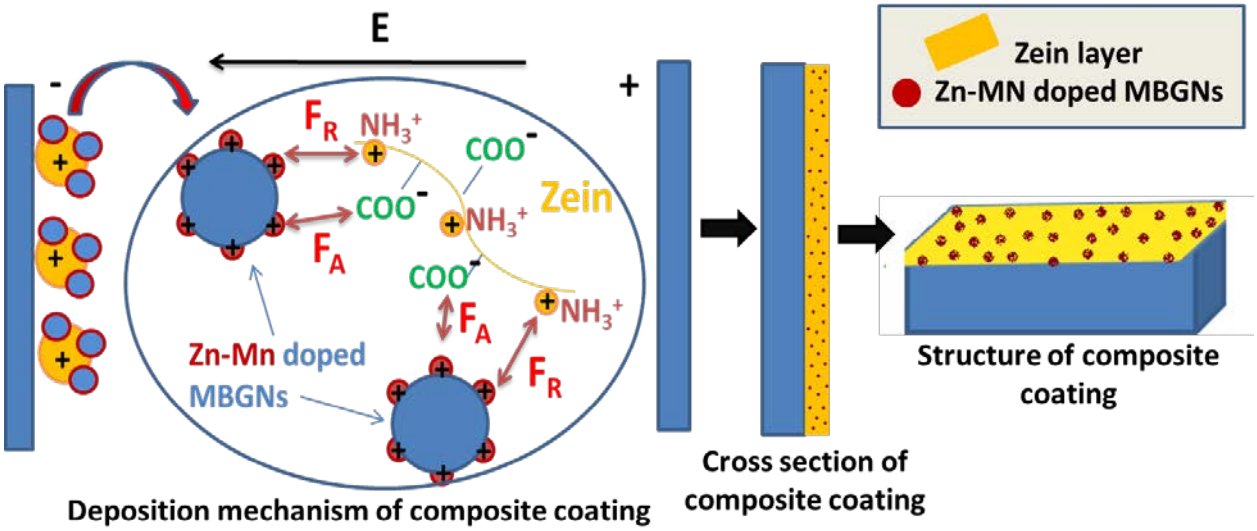

Figure 3. Deposition and stabilization mechanism of zein/Zn-Mn MBGNs suspension.

3.3. Deposition mechanism of zein/Zn-Mn doped MBGNs

In acidic environment, zein has positive charge due to which it moves towards cathode. The pKa value (acidic dissociation constant) for zein is 18.6 (Source: ChemAxon). The pKa value determines the solubility of the molecules in an acidic or basic medium. If the pH of the suspension is lower than its pKa value, then zein is soluble in solution and vice versa.

In zein, polar and non-polar functional groups are present. In the highly concentrated solutions of ethanol (>90 %) the protonation of zein occurs which leads to the deposition of zein molecules on cathode. However, if ethanol solution is less concentrated (<90 %) then zein gets negatively charged and migrates towards the anode. Hence there is a possibility to manipulate the deposition of the zein molecules on either anode or cathode [19,35,56]. As the ethanol used in this study is absolute (99 %), cathodic deposition takes place due to the protonation of zein molecules. Meyer et al. [57] suggested the deposition of zein/BG composite particles on cathode could be due to the bonding of the hydrophilic side groups of zein with BG particles and their co-migration towards the cathode.

When the voltage is applied, a reduction reaction occurs near the cathode. Here the local pH increases due to the production of hydrogen and hydroxyl ions. The amine group of zein is protonated in the aqueous medium (H_3O^+). The ammonium (NH_3^+) group of zein then migrates towards the negative electrode and reacts with hydroxyl ions at cathode. As a result, the charge on the amine group of zein is lost and it gets deposited on cathode along with Zn-Mn MBGNs. Sarkar et al. [58] also explained the deposition mechanism in consequence of charge neutralization.

Preprints (www.preprints.org) | NOT PEER-REVIEWED | Posted: 27 June 2022 doi:10.20944/preprints202206.0352.v1

3.4. EPD of zein/Zn-Mn MBGNs (DoE approach)

The best operating parameters for EPD and suspension concentration were obtained via Taguchi DoE method. The method elucidated the maximum attainable deposition yield with minimum standard deviation. For the coatings to be applied on orthopedic implants, it is important to maximize their bioactivity. The bioactive behavior of a coating material is the key parameter which determines the ability of an orthopedic implant to bond with soft and hard tissues [5]. Therefore, the zein suspension with high concentration of Zn-Mn MBGNs will result in high deposition yield, thus increasing bioactivity of the coating in physiological environment. MBGNs form a hydroxyapatite (HA) layer over its surface on contact with body fluid. HA layer is bioactive and is known to induce osteoconductivity [59]. The co-doping of the Zn and Mn metallic ions provides synergetic effect. Zn is proven to be an excellent antibacterial agent thus it will hinder the formation of biofilm on the implant [39,60]. Furthermore, Mn is an excellent osteogenic material widely used in bone tissue engineering [24,61].

Figure 4 shows the change in the deposition yield of zein/Zn-Mn MBGNs coatings with respect to the levels of control factors. Figure 4A and B display the values of mean of means deposition yield and mean S/N deposition yield. The maximum values are obtained at A4 (20 V), B4 (7 min) and C4 (4 g/L of Zn-Mn MBGNs) in both cases. It confirms that there is no notable difference in the response of mean deposition yield and mean S/N deposition yield values. The deposition rate increase with the increase in applied voltage, time and conc. of Zn-Mn MBGNs in zein suspension. This is in complete agreement with Hamaker's law [52].

In terms of standard deviation, the minimum values are obtained at A4 (20 V), B3 (5 min), and C4 (4 g/L of Zn-Mn MBGNs) as shown in Figure 4C. Figure 4D shows that maximum values of mean S/N ratio for standard deviation are A1 (5 V), B1 (1 min), C1 (1 g/L of Zn-Mn MBGNs). Thus the best parameters in terms of standard deviation are A4, B3, and C4.

Preprints (www.preprints.org) | NOT PEER-REVIEWED | Posted: 27 June 2022 doi:10.20944/preprints202206.0352.v1

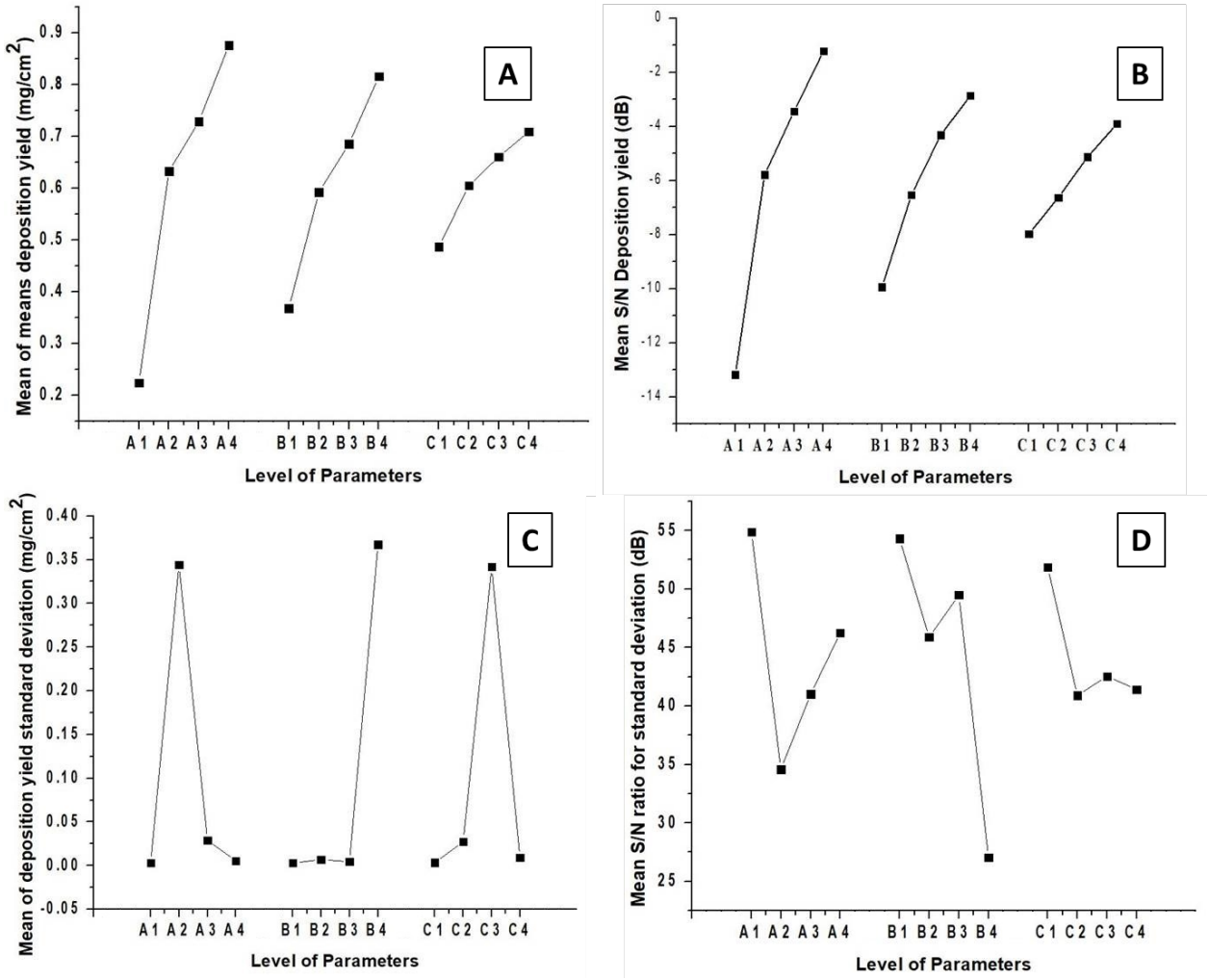

Figure 4. Effect of control parameters on the deposition yield of zein/Zn-Mn MBGNs coating produced by EPD: (A) mean of means deposition yield, (B) mean S/N deposition yield, (C) mean of deposition yield standard deviation, and (D) mean S/N ratio for standard deviation.

The parameters selected from standard deviation values are comparable with the mean deposition yield values. Therefore, there is a need to compromise on certain parameters. Since these coatings require high deposition yield, preference is given to the coatings which are deposited with high conc. of Zn-Mn MBGNs. According to the maximum-minimum values presented in Table 4 for S/N response for deposition yield, voltage is the most effective factor to determine the deposition yield. In case of S/N response to standard deviation, maximum-minimum values shown in Table 5 infer that conc. of Zn-Mn MBGNs is most effective parameter. For the parameter B4 (7 min) standard deviation and S/N response to standard deviation for deposition yield is very high. Therefore, it is concluded that the best parameters are A4 (20 V), B3 (5 min), and C4 (conc. of Zn-Mn doped MBGNs: 4 g/L of Zn-Mn MBGNs).

Table 4. S/N (dB) response for deposition yield of zein/Zn-Mn MBGNs coating.

Factors	Level 1	Level 2	Level 3	Level 4	Δ=Max.-Min.
Voltage (V)	-13.181	-5.785	-3.450	-1.223	11.958
Time (min)	-9.934	-6.527	-4.316	-2.862	7.072
Conc. of Zn-Mn MBGNs (g/L)	-7.977	-6.632	-5.124	-3.906	4.071

Preprints (www.preprints.org) | NOT PEER-REVIEWED | Posted: 27 June 2022 doi:10.20944/preprints202206.0352.v1

Table 5. S/N (dB) response to standard deviation for deposition yield of zein/Zn-Mn MBGNs coating.

Factors	Level 1	Level 2	Level 3	Level 4	Δ=Max.-Min.
Voltage (V)	54.89	34.57	41.01	46.24	20.32
Time (min)	54.31	45.88	49.49	27.04	27.26
Conc. of Zn-Mn MBGNs (g/L)	51.86	40.90	42.54	41.42	10.96

3.5. Morphological analysis of zein/Zn-Mn MBGNs coating

The coatings were prepared using optimized EPD parameters (20 V, 5 min and 4 g/L Zn-Mn MBGNs) obtained by Taguchi DoE approach. At first, the coatings were analyzed using an optical microscope. The optical microscope showed a uniform covering of 316L SS substrate by the zein/Zn-Mn MBGNs coating. For in-depth understanding of the surface morphology SEM analysis was performed. Figure 5 (A and B) show the SEM micrographs at low and high magnifications, respectively. It was clearly seen that a homogeneous coating of zein/Zn-Mn MBGNs was produced at 20 V, 5 min and 4 g/L conc. of Zn-Mn MBGNs. Zn-Mn MBGNs were seen uniformly dispersed throughout the zein matrix as shown in Figure 5A. However, at some points few Zn-Mn MBGNs were found in the form of agglomerates. Cross sectional SEM image (Figure 5C) of the coating show that deposited film had a uniform thickness of ≈18 µm. Figure 5D shows the elemental mapping of the coating from cross-section. The red and green colored area attributed to the Fe and Cr representing 316L SS whereas purple, orange and dark green represent constituents of composite coating i.e. Si, Ca and C, respectively. EDS analysis was also performed to determine the composition of composite coating qualitatively. The presence of Si, Ca, Zn, and Mn was evident from EDS spectrum as shown in Figure 5E. The elemental mapping validated EDS spectrum. For further affirmation of the presence of zein/Zn-Mn MBGNs in the composite coating, FTIR was carried out.

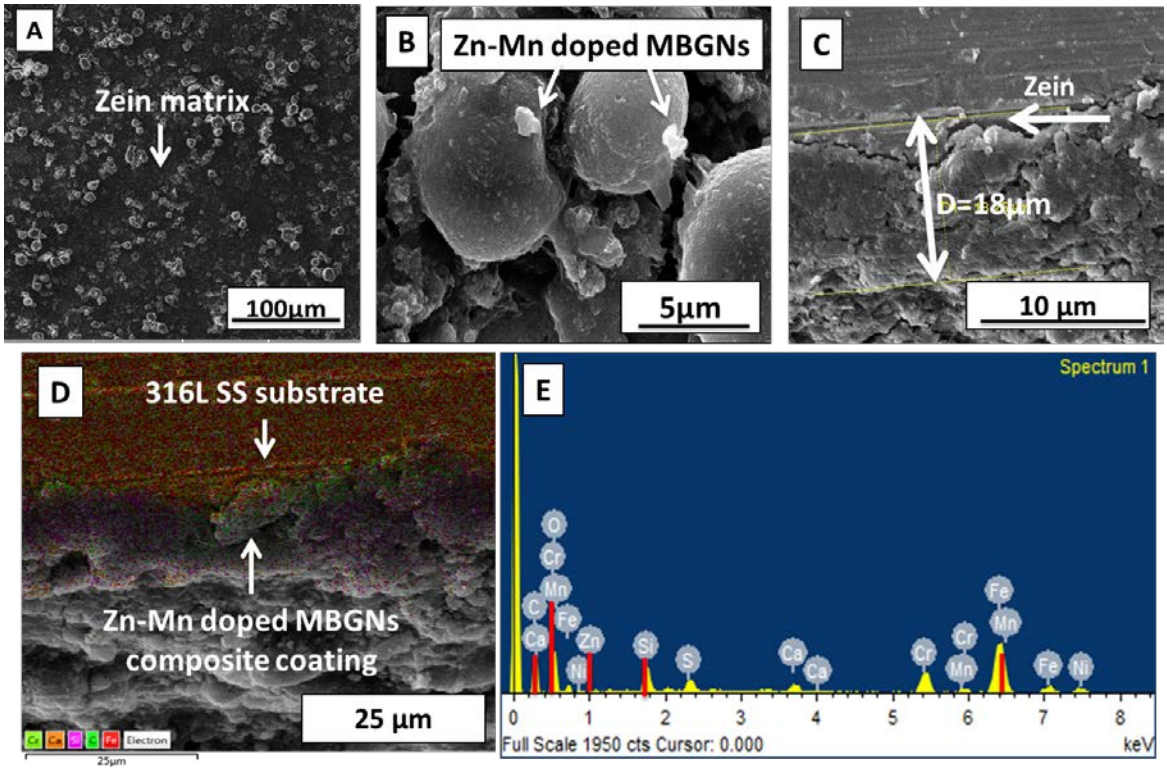

Preprints (www.preprints.org) | NOT PEER-REVIEWED | Posted: 27 June 2022 doi:10.20944/preprints202206.0352.v1

Figure 5. SEM images of zein/Zn-Mn MBGNs coatings produced at 20 V, 5 min, (A) low magnification showing uniform deposition of the coating, (B) high magnification showing distribution of Zn-Mn MBGNs on zein particles, (C) cross section, (D) elemental mapping, and (E) EDS spectrum of composite coating.

3.6. FTIR analysis of zein/Zn-Mn MBGNs coating

FTIR analysis monitors the interaction of molecules during EPD. It also evaluates the conformational variations occurring during the deposition process [33]. Amide groups (I and II) of amino acids can be easily detected by FTIR.

Figure 6 shows the FTIR spectrum of zein/Zn-Mn MBGNs composite coating in the range of 2000-500 cm^{-1}. The characteristic peaks of zein and Zn-Mn MBGNs were determined as shown in Table 6.

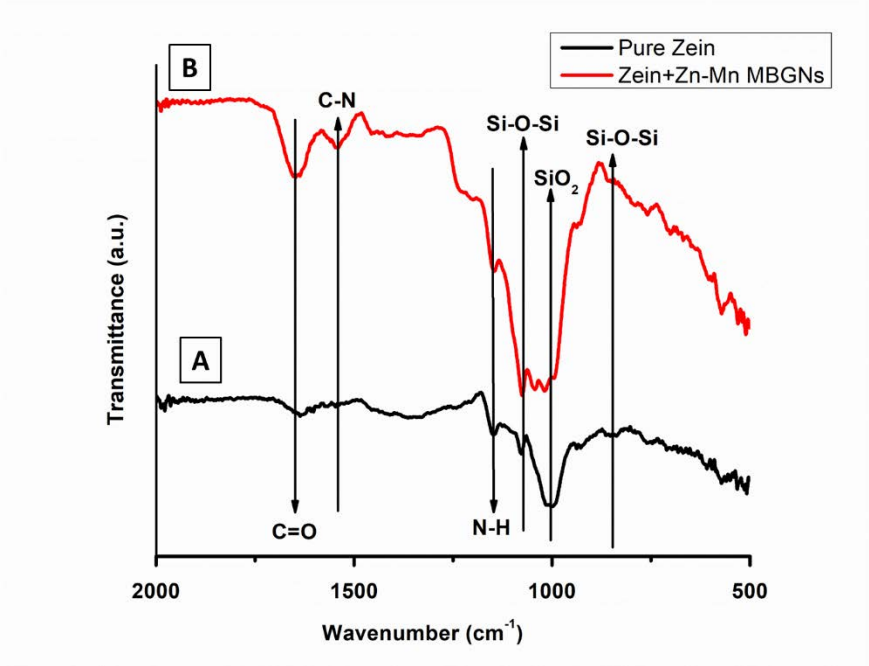

Figure 6. FTIR spectrum of (A) pure zein, and (B) composite coating.

Table 6. Characteristic FTIR peaks of pure zein and composite coating.

Wave numbers (cm^{-1})	Associated bonds	Material	References
800	Si-O-Si	Zn-Mn MBGNs	[57,62]
1040	SiO_2	Zn-Mn MBGNs	[57,62]
1067	Si-O-Si	Zn-Mn MBGNs	[62]
1230	N-H	Zein	[57,62]
1510	C-N	Zein	[57,62,63]
1650	C=O	Zein	[57,62,63]
2919	C-H	Zein	[57,62,63]
3292	O-H	Zein	[57,62,63]

Pure zein represented characteristics peaks of amide I (C=O), II (C-N) and III (N-H) at 1590 cm^{-1}, 1410 cm^{-1}, and 1230 cm^{-1}, respectively. After incorporating Zn-Mn MBGNs in zein, a similar pattern was observed in FTIR spectrum. The peaks attributed to the MBGNs were prominent at 800 cm^{-1} (Si-O-Si), 1040 cm^{-1} (SiO_2), and 1067 cm^{-1} (Si-O-Si). The overlapping peaks in the region of 1000 cm^{-1} to 1700 cm^{-1} confirmed the formation of hydrogen bonding between zein and Zn-Mn doped MBGNs. Due to strong hydrogen bonding between zein and MBGNs the composite coating showed excellent adhesion results (discussed in next sections).

Preprints (www.preprints.org) | NOT PEER-REVIEWED | Posted: 27 June 2022 doi:10.20944/preprints202206.0352.v1

3.7. Surface roughness test

Surface roughness is an important factor to consider for microbial and cell attachment. It greatly affects the performance of an implant material as the surface is the first thing that comes in contact with body fluids. According to the literature, osteoblasts attach with a surface having roughness range of 1-2 μm [64]. In the present study, R_a for composite coating was higher (1.8 μm) than pure zein (1.2 μm) coating. This could be due to the incorporation of Zn-Mn MBGNs in the zein suspension. Our previous studies also confirm the increased R_a value after adding MBGNs in polymer coatings [24,65].

3.8. Wettability test for zein/Zn-Mn MBGNs coating

The wetting property of a coating determines the ability to facilitate protein adsorption at the surface. In ideal situation, surface should not be fully hydrophilic or hydrophobic. CA range of 35°-80° is considered suitable for excellent cell adhesion and proliferation [30]. The water CA was measured for 316L SS, pure zein coating and zein/Zn-Mn MBGNs composite coating. The 316L SS presented the CA value of 58 ± 6°. Pure zein showed average CA value of 63 ± 4° and for composite coating itwas measured as 80 ± 9°. The CA for pure zein was slightly higher than that of 316L SS. As the chemical structure of zein (shown in Figure 4) depicts that it has both hydrophilic and hydrophobic side groups, it is quite possible that hydrophilic groups of zein were oriented towards the top of the surface during deposition offering more attraction to the water drop. The CA of composite coating was even higher than 316L SS and pure zein coating. Although, addition of MBGNs augments the hydrophobic character of composite coating still this value is in the suitable range for protein adsorption and spreading. Similar results were reported by Mariotti et al. [66]. An increment in CA value was observed after incorporating Cu doped BGs in the zein fiber mat.

3.9. Adhesion of zein/Zn-Mn MBGNs coating

Tape adhesion test was performed on composite coating to assess the response of coating towards mechanical stresses. The composite coating was inspected under an optical microscope. Figure 7 shows the optical images of the composite coating before (Figure 7A) and after (Figure 7B) removing tape. The composite coating clearly showed very little (<5%) delamination after removing tape. Considering these results the adhesion strength was graded '4B' according to the ASTM standard.

Tensile test for composite coatings was performed according to the ASTM D3039 [67]. The 316L SS rectangular plates joined with epoxy were detached at 55 MPa (7C) whereas the set of uncoated and coated plates showed detachment at 46 MPa (7D). It was observed that 316L SS had good adhesion with epoxy thus epoxy film was split on both sheets. However, the epoxy was detached from the composite coating side for the other set. A little amount of epoxy was still adhered with coated sheet 2 whereas no sign of detached composite coating was visible on epoxy. This test concluded that composite coating was well adhered with substrate.

To further analyze the scratch resistance of coatings, pencil hardness test was performed. The scratching was started from hard grade (2H) pencil and was continued down towards softer grades at the hardness scale (2H-8B). The samples were subjected to test until the pencil could no further scratch the coating. For each type of coating, test was performed on three samples and results were compared with ASTM standard. It was revealed that pure zein coating had a hardness grade of '7B' (soft) whereas composite coating showed a hardness of '4B' (hard). The higher hardness value of composite coating was attributed to the strong adhesion of coating with substrate.

The coatings were also subjected to 180° bend manually as shown in Figure 7 (E & F). It was observed that both coatings were strongly adhered to the substrate and no sign of delamination was seen. The coatings were rated '4B' according to the ASTM standard.

Preprints (www.preprints.org) | NOT PEER-REVIEWED | Posted: 27 June 2022 doi:10.20944/preprints202206.0352.v1

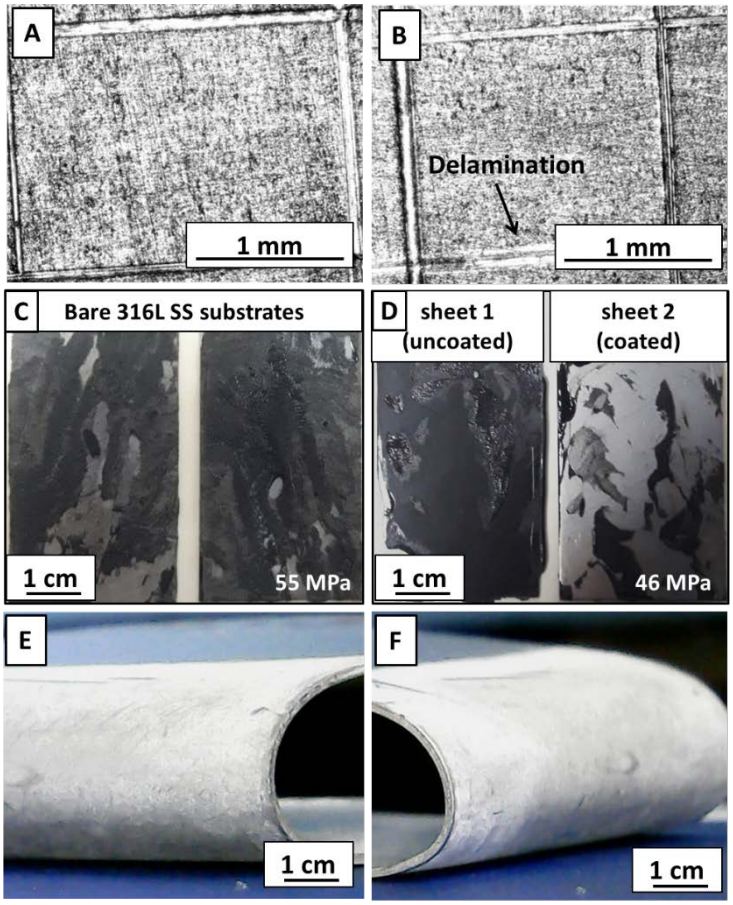

Figure 7. Tape test on composite coating: (A) before and (B) after removing tape, Tensile test: (C) detached bare 316L SS sheets and (D) bare 316L SS sheet 1 detached from coated sheet 2, Bend test: (E) pure zein coating, and (F) composite coating without any cracks.

To realize a successful implantation in the physical environment it is necessary to examine the wear behavior of coatings. Wear resistance also infers that how an implant material will react towards somewhat vigorous handling of implant during surgical procedures. To confirm the suitability of composite coating, wear study was carried out. Figure 8 shows partial wear tracks of pure zein (Figure 8a) and composite coating (Figure 8b) observed under optical microscope. Pure zein coating was removed almost completely after test whereas composite coating was still intact at some points. The coefficient of friction (CoF) throughout the sliding distance was same for both coatings (Figure 8A and B). Figure 8C shows the wear rate of both types of coatings. It is evident that pure zein coating has higher wear rate as compared to the composite coating. The better wear resistance of composite coating could be due to the presence of MBGNs owing to the fact that BG belongs to the class of rigid bioceramics. This affirms their suitability for implant coating.

Preprints (www.preprints.org) | NOT PEER-REVIEWED | Posted: 27 June 2022 doi:10.20944/preprints202206.0352.v1

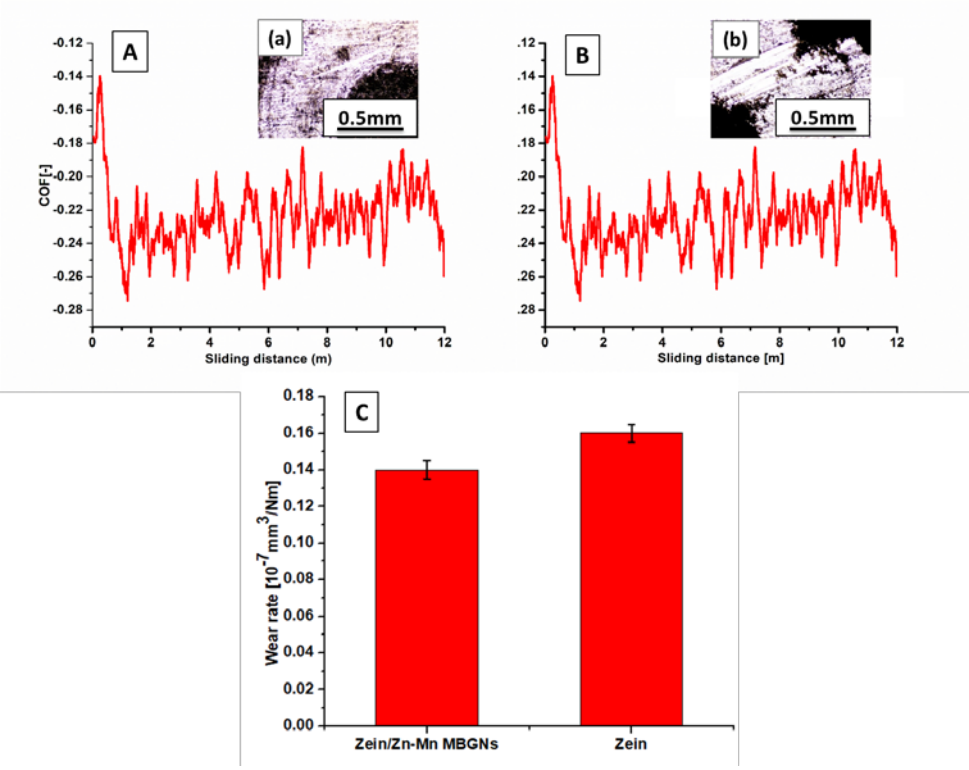

Figure 8. Graphs showing the CoF Vs. sliding distance curves for (A) pure zein coating, (B) composite coating, (C) wear rate of pure zein and composite coatings. Wear track images taken from optical microscope (a) pure zein, (b) composite coating.

3.10. Corrosion behavior of zein/Zn-Mn MBGNs coating

The potentiodynamic polarization curves of bare 316L SS and zein/Zn-Mn MBGNs coated samples are given in Figure 9. The anodic polarization curve depicts the dissolution of iron and other alloying elements from 316L SS into respective ions. The cathodic branch of polarization curve shows the hydrogen evolution. Bare sample shows more abrupt significant increase in corrosion potential in passive region as compare to coated sample, which is attributed to the rapid dissolution of substrate. The measured E_{corr} and I_{corr} values are given in the inset of the Figure 9. It shows that I_{corr} value for composite coating has decreased ~100 turns. Therefore, the coating can improve the corrosion resistance of 316L SS.

Preprints (www.preprints.org) | NOT PEER-REVIEWED | Posted: 27 June 2022 doi:10.20944/preprints202206.0352.v1

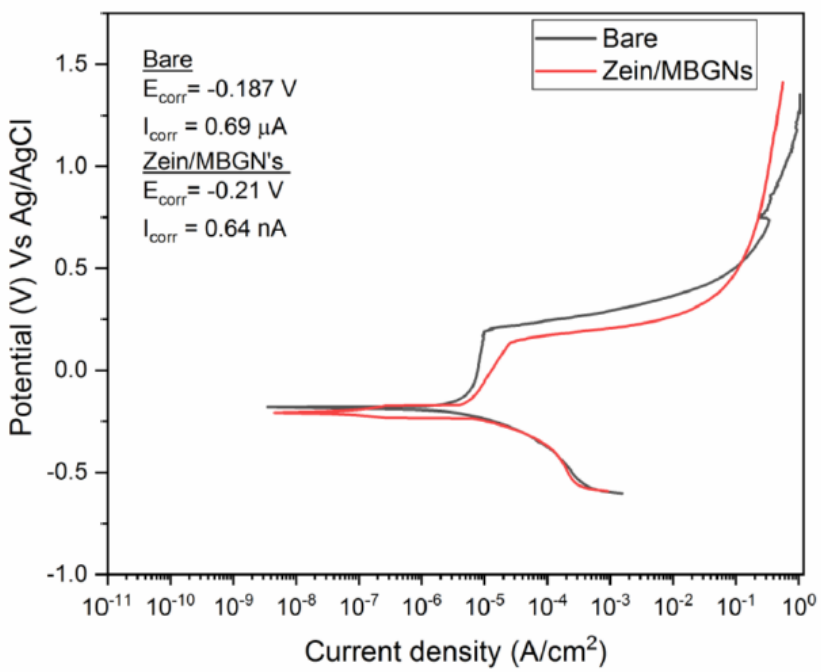

Figure 9. Potentiodynamic curve for base 316L SS and zein/Zn-Mn MBGNs coatings.

3.11. Antibacterial analysis (CFU)

Zein/Zn-Mn MBGNs coated sample was tested against the *S. aureus* and *E. coli*. The bacterial growth on control plates was maximum as shown in Figure 10 (A & B). The coating effectively inhibited the growth of bacteria. It was observed that the coating fully inhibited the growth of *S. aureus* and zero CFU was attained (Figure 10 C). Whereas, partial inhibition was observed in case of *E. coli* (Figure 10D). However, the colonies were in countable range. The bacterial inhibition is attributed to the presence of Zn in MBGNs which is a strong antibacterial agent. The antibacterial effect also affirms the release of Zn-ion in the solution.

Preprints (www.preprints.org) | NOT PEER-REVIEWED | Posted: 27 June 2022 doi:10.20944/preprints202206.0352.v1

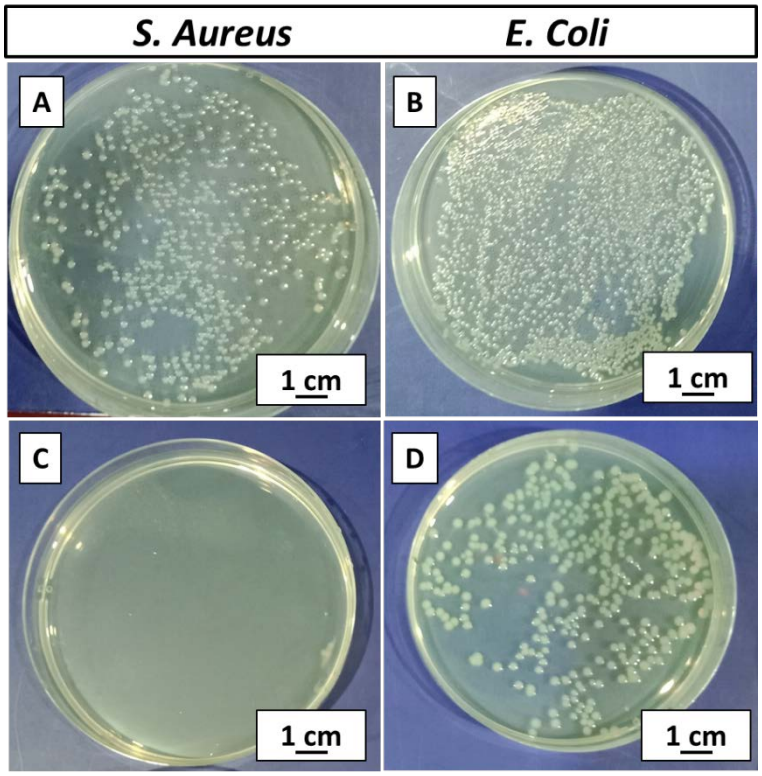

Figure 10. CFU results for zein/Zn-Mn MBGNs composite coating, (A) Control (*S. aureus*), (B) Control (*E. coli*), (C) complete inhibition of *S. aureus*, and (D) partial inhibition of *E. coli*.

3.12. In-vitro bioactivity test for zein/Zn-Mn MBGNs coating

The in-vitro bioactivity test was carried out for zein/Zn-Mn MBGNs composite coating for 1, 2, 3, 5, and 7 days of incubation. SEM/EDX analysis performed at day 3 confirmed the formation of cauliflower like HA structure on the surface coating as shown in Figure 11. It was observed that HA started to form at day 3 (Figure 11A) as the composition of BG used in this study was composed of SiO_2 and CaO in the ratio of 70:30 without any addition of phosphorous (P). Thus the delayed formation of HA could be due to absence of P in the BG. However, HA was formed which proved the bioactivity of composite coating. Figure 11B shows the EDX spectra of HA layer consisting of Ca and P.

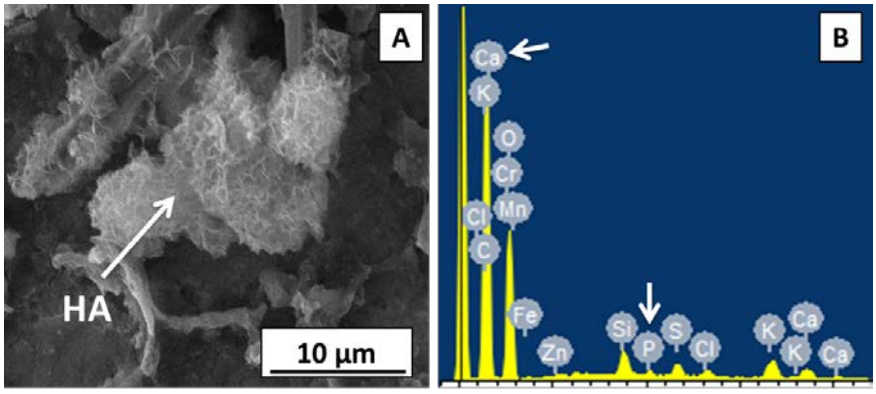

Figure 11. SEM/EDX analysis of composite coating after treating in SBF for 3 days (A) formation of cauliflower like HA structure, (B) detection of Ca and P confirms the presence of HA.

4. Conclusions

Following conclusions were drawn from the present study.

1. Zein/Zn-Mn MBGNs composite coatings were deposited via EPD on 316L SS.

Preprints (www.preprints.org) | NOT PEER-REVIEWED | Posted: 27 June 2022 doi:10.20944/preprints202206.0352.v1

2. The optimized parameters were obtained from Taguchi DoE approach by running an array of experiments. The experiments deduced that coatings deposited at 20 V for 5 min with 4 g/L conc. of Zn-Mn MBGNs in zein suspension resulted in high deposition yield.
3. SEM/EDX analysis confirmed a uniform composite coating of thickness ≈18µm.
4. FTIR verified the hydrogen bonding of zein polymer with Zn-Mn MBGNs which resulted in augmented adhesion strength of composite coating with substrate.
5. The surface roughness and wettability analysis affirmed the possibility of cell attachment and growth on composite coatings.
6. For adhesion, tape test, bend test, pencil hardness test, tensile test and wear test were carried out. The tests displayed favorable results according to the ASTM standards.
7. Corrosion behavior analysis of composite coatings showed that appreciable corrosion resistance was achieved.
8. CFU test revealed the efficacy of Zn-Mn MBGNs in the zein coating against *S. aureus* and *E. coli*.
9. Zein/Zn-Mn MBGNs composite coatings formed hydroxyapatite structure in SBF proving osteogenic potential of the composite coatings in bone tissue engineering.

References

1. Ahmed, Y.; Yasir, M.; Atiq, M.; Rehman, U. Fabrication and Characterization of Zein / Hydroxyapatite Composite Coatings for Biomedical Applications. **2020**, 237–250.

2. Wang, W.; Yeung, K.W.K.K. Bone Grafts and Biomaterials Substitutes for Bone Defect Repair: A Review. *Bioact. Mater.* **2017**, *2*, 224–247, doi:10.1016/j.bioactmat.2017.05.007.

3. Chew, K.-K.; Zein, S.H.S.; Ahmad, A.L. The Corrosion Scenario in Human Body: Stainless Steel 316L Orthopaedic Implants. *Nat. Sci.* **2012**, *04*, 184–188, doi:10.4236/ns.2012.43027.

4. Eliaz, N. Corrosion of Metallic Biomaterials: A Review. *Mater. (Basel, Switzerland)* **2019**, *12*, 407, doi:10.3390/ma12030407.

5. Goldmann, W.H. Biosensitive and Antibacterial Coatings on Metallic Material for Medical Applications. *Cell Biol. Int.* **2021**, *n/a*, doi:https://doi.org/10.1002/cbin.11604.

6. Wang, Z.; Thian, E.S.; Li, X.; Best, S. Bio-Responsive Materials for Tissue Regeneration. *J. Phys. Mater.* **2020**, *3*, 20201, doi:10.1088/2515-7639/ab6d3f.

7. Gaharwar, A.K.; Singh, I.; Khademhosseini, A. Engineered Biomaterials for in Situ Tissue Regeneration. *Nat. Rev. Mater.* **2020**, *5*, 686–705, doi:10.1038/s41578-020-0209-x.

8. Ghasemlou, M.; Daver, F.; Ivanova, E.P.; Rhim, J.-W.; Adhikari, B. Switchable Dual-Function and Bioresponsive Materials to Control Bacterial Infections. *ACS Appl. Mater. Interfaces* **2019**, *11*, 22897–22914, doi:10.1021/acsami.9b05901.

9. Ramos, L.; Cochis, A.; Biser, S.; Canciani, E.; Ferraris, S.; Rimondini, L.; Boccaccini, A.R. Bioactive Materials Copper Based Coatings for Implantable Stainless Steel Aimed at Bone Healing. *Bioact. Mater.* **2021**, *6*, 1479–1490, doi:10.1016/j.bioactmat.2020.11.001.

10. Ferraris, S.; Yamaguchi, S.; Barbani, N.; Cazzola, M.; Cristallini, C.; Miola, M.; Vernè, E.; Spriano, S. Bioactive Materials:

Preprints (www.preprints.org) | NOT PEER-REVIEWED | Posted: 27 June 2022 doi:10.20944/preprints202206.0352.v1

In Vitro Investigation of Different Mechanisms of Hydroxyapatite Precipitation. *Acta Biomater.* **2020**, *102*, 468–480, doi:https://doi.org/10.1016/j.actbio.2019.11.024.

11. Florea, D.A.; Albuleț, D.; Grumezescu, A.M.; Andronescu, E. Surface Modification – A Step Forward to Overcome the Current Challenges in Orthopedic Industry and to Obtain an Improved Osseointegration and Antimicrobial Properties. *Mater. Chem. Phys.* **2020**, *243*, 122579, doi:https://doi.org/10.1016/j.matchemphys.2019.122579.

12. Mansoorianfar, M.; Mansourianfar, M.; Fathi, M.; Bonakdar, S.; Ebrahimi, M.; Zahrani, E.M.; Hojjati-Najafabadi, A.; Li, D. Surface Modification of Orthopedic Implants by Optimized Fluorine-Substituted Hydroxyapatite Coating: Enhancing Corrosion Behavior and Cell Function. *Ceram. Int.* **2020**, *46*, 2139–2146, doi:https://doi.org/10.1016/j.ceramint.2019.09.197.

13. Arora, D.; Pant, P.; Sharma, P.K. Trends in Functional Biomaterials in Tissue Engineering and Regenerative Medicine BT - Biomaterials in Tissue Engineering and Regenerative Medicine: From Basic Concepts to State of the Art Approaches. In; Bhaskar, B., Sreenivasa Rao, P., Kasoju, N., Nagarjuna, V., Baadhe, R.R., Eds.; Springer Singapore: Singapore, 2021; pp. 215–269 ISBN 978-981-16-0002-9.

14. Shukla, R.; Cheryan, M. Zein: The Industrial Protein from Corn. *Ind. Crops Prod.* **2001**, *13*, 171–192, doi:https://doi.org/10.1016/S0926-6690(00)00064-9.

15. Müller, V.; Piai, J.F.; Fajardo, A.R.; Fávaro, S.L.; Rubira, A.F.; Muniz, E.C. Preparation and Characterization of Zein and Zein-Chitosan Microspheres with Great Prospective of Application in Controlled Drug Release. *J. Nanomater.* **2011**, *2011*, 928728, doi:10.1155/2011/928728.

16. Paliwal, R.; Palakurthi, S. Zein in Controlled Drug Delivery and Tissue Engineering. *J. Control. Release* **2014**, *189*, 108–122, doi:10.1016/j.jconrel.2014.06.036.

17. Arango-Ospina, M.; Lasch, K.; Weidinger, J.; Boccaccini, A.R. Manuka Honey and Zein Coatings Impart Bioactive Glass Bone Tissue Scaffolds Antibacterial Properties and Superior Mechanical Properties. *Front. Mater.* **2021**, *7*, 449, doi:10.3389/fmats.2020.610889.

18. Batool, S.A.; Wadood, A.; Hussain, S.W.; Yasir, M.; Ur Rehman, M.A. A Brief Insight to the Electrophoretic Deposition of PEEK-, Chitosan-, Gelatin-, and Zein-Based Composite Coatings for Biomedical Applications: Recent Developments and Challenges. *Surfaces* 2021, *4*.

19. Ramos Rivera, L.; Dippel, J.; Boccaccini, A.R. Formation of Zein/Bioactive Glass Layers Using Electrophoretic Deposition Technique. *ECS Trans.* **2018**, *82*, 73–80, doi:10.1149/08201.0073ecst.

20. Ahmed, Y.; Ur Rehman, M.A. Improvement in the Surface Properties of Stainless Steel via Zein/Hydroxyapatite Composite Coatings for Biomedical Applications. *Surfaces and Interfaces* **2020**, *20*, 100589,

Preprints (www.preprints.org) | NOT PEER-REVIEWED | Posted: 27 June 2022 doi:10.20944/preprints202206.0352.v1

doi:https://doi.org/10.1016/j.surfin.2020.100589.

21. Atiq, M.; Rehman, U. Zein / Bioactive Glass Coatings with Controlled Degradation of Magnesium under Physiological Conditions : Designed for Orthopedic Implants. **2020**, 211–224.

22. Lim, P.N.; Tong, S.Y.; Ho, B.; Wang, W.; Thian, E.S. A Functional Apatite with Antibacterial Efficacy for Bone Tissue Infections. *J. Phys. Mater.* **2019**, *2*, 34004, doi:10.1088/2515-7639/ab1207.

23. Ur Rehman, M.A.; Ferraris, S.; Goldmann, W.H.; Perero, S.; Bastan, F.E.; Nawaz, Q.; Confiengo, G.G. Di; Ferraris, M.; Boccaccini, A.R. Antibacterial and Bioactive Coatings Based on Radio Frequency Co-Sputtering of Silver Nanocluster-Silica Coatings on PEEK/Bioactive Glass Layers Obtained by Electrophoretic Deposition. *ACS Appl. Mater. Interfaces* **2017**, *9*, 32489–32497, doi:10.1021/acsami.7b08646.

24. Nawaz, A.; Bano, S.S.S.; Yasir, M.; Wadood, A.; Atiq, M.; Rehman, U.; Ur Rehman, M.A.; Rehman, M.A.U. Ag-Mn Doped Mesoporous Bioactive Glass Nanoparticles in Corporated into the Chitosan/Gelatin Coatings Deposited on PEEK / Bioactive Glass Layers for Favorable Osteogenic Differentiation and Antibacterial Activity Materials Advances. *Mater. Adv.* **2020**, *1*, 1273–1284, doi:10.1039/d0ma00325e.

25. Saleem, O.; Wahaj, M.; Akhtar, M.A.; Ur Rehman, M.A. Fabrication and Characterization of Ag-Sr-Substituted Hydroxyapatite/Chitosan Coatings Deposited via Electrophoretic Deposition: A Design of Experiment Study. *ACS Omega* **2020**, *5*, 22984–22992, doi:10.1021/acsomega.0c02582.

26. Li, Y.; Ho, J.; Ooi, C.P. Antibacterial Efficacy and Cytotoxicity Studies of Copper (II) and Titanium (IV) Substituted Hydroxyapatite Nanoparticles. *Mater. Sci. Eng. C* **2010**, *30*, 1137–1144, doi:https://doi.org/10.1016/j.msec.2010.06.011.

27. Seuss, S.; Heinloth, M.; Boccaccini, A.R. Development of Bioactive Composite Coatings Based on Combination of PEEK, Bioactive Glass and Ag Nanoparticles with Antibacterial Properties. *Surf. Coatings Technol.* **2015**, *301*, 100–105, doi:10.1016/j.surfcoat.2016.03.057.

28. Boccaccini, A.R.; Keim, S.; Ma, R.; Li, Y.; Zhitomirsky, I. Electrophoretic Deposition of Biomaterials. *J. R. Soc. Interface* **2010**, *7*, doi:10.1098/rsif.2010.0156.focus.

29. Ferrari, B.; Moreno, R. EPD Kinetics: A Review. *J. Eur. Ceram. Soc.* **2010**, *30*, 1069–1078, doi:10.1016/j.jeurceramsoc.2009.08.022.

30. Maci, F.; Moskalewicz, T.; Kowalski, K.; Łukaszczyk, A.; Hadzhieva, Z.; Boccaccini, A.R. The Effect of Electrophoretic Deposition Parameters on the Microstructure and Adhesion of Zein Coatings to Titanium Substrates. **2021**.

31. Al-Dawalibi, A.; Al-Dali, I.H.; Alkhayyal, B.A. Best Marketing Strategy Selection Using Fractional Factorial Design with Analytic Hierarchy Process. *MethodsX* **2020**, *7*, 100927, doi:https://doi.org/10.1016/j.mex.2020.100927.

Preprints (www.preprints.org) | NOT PEER-REVIEWED | Posted: 27 June 2022 doi:10.20944/preprints202206.0352.v1

32. Terzyk, A.P.; Zięba, M.; Koter, S.; Korczeniewski, E.; Zięba, W.; Kowalczyk, P.; Kujawa, J. Recent Developments in the Electrophoretic Deposition of Carbon Nanomaterials BT - Porous Materials: Theory and Its Application for Environmental Remediation. In; Moreno-Piraján, J.C., Giraldo-Gutierrez, L., Gómez-Granados, F., Eds.; Springer International Publishing: Cham, 2021; pp. 113–137 ISBN 978-3-030-65991-2.

33. Rehman, M.A.U.; Munawar, M.A.; Schubert, D.W.; Boccaccini, A.R. Electrophoretic Deposition of Chitosan/Gelatin/Bioactive Glass Composite Coatings on 316L Stainless Steel: A Design of Experiment Study. *Surf. Coatings Technol.* **2019**, *358*, 976–986, doi:10.1016/j.surfcoat.2018.12.013.

34. Atiq Ur Rehman, M.; Bastan, F.E.; Haider, B.; Boccaccini, A.R.; Rehman, M.A.U.; Bastan, F.E.; Haider, B.; Boccaccini, A.R. Electrophoretic Deposition of PEEK/Bioactive Glass Composite Coatings for Orthopedic Implants: A Design of Experiments (DoE) Study. *Mater. Des.* **2017**, *130*, 223–230, doi:https://doi.org/10.1016/j.matdes.2017.05.045.

35. Kaya, S.; Boccaccini, A.R. Electrophoretic Deposition of Zein Coatings. *J. Coatings Technol. Res.* **2017**, *14*, 683–689.

36. Bekmurzayeva, A.; Duncanson, W.J.; Azevedo, H.S.; Kanayeva, D. Surface Modification of Stainless Steel for Biomedical Applications: Revisiting a Century-Old Material. *Mater. Sci. Eng. C* **2018**, *93*, 1073–1089, doi:https://doi.org/10.1016/j.msec.2018.08.049.

37. Zhang, E.; Zhao, X.; Hu, J.; Wang, R.; Fu, S.; Qin, G. Antibacterial Metals and Alloys for Potential Biomedical Implants. *Bioact. Mater.* **2021**, *6*, 2569–2612, doi:https://doi.org/10.1016/j.bioactmat.2021.01.030.

38. Bano, S.; Akhtar, M.; Yasir, M.; Maqbool, M.S.; Niaz, A.; Wadood, A.; Atiq, M.; Rehman, U. Synthesis and Characterization of Silver–Strontium (Ag-Sr)-Doped Mesoporous Bioactive Glass Nanoparticles. *Gels* **2021**, *7*, 1–15, doi:https://doi.org/10.3390/gels7020034.

39. Westhauser, F.; Decker, S.; Nawaz, Q.; Rehder, F.; Wilkesmann, S.; Moghaddam, A.; Kunisch, E.; Boccaccini, A.R. Impact of Zinc- or Copper-Doped Mesoporous Bioactive Glass Nanoparticles on the Osteogenic Differentiation and Matrix Formation of Mesenchymal Stromal Cells. *Mater. (Basel, Switzerland)* **2021**, *14*, doi:10.3390/ma14081864.

40. Li, W.; Zhao, D. Extension of the Stöber Method to Construct Mesoporous SiO2 and TiO2 Shells for Uniform Multifunctional Core–Shell Structures. *Adv. Mater.* **2013**, *25*, 142–149, doi:https://doi.org/10.1002/adma.201203547.

41. Beddoes, J.; Bucci, K. The Influence of Surface Condition on the Localized Corrosion of 316L Stainless Steel Orthopaedic Implants. *J. Mater. Sci. Mater. Med.* **1999**, *10*, 389–394, doi:10.1023/A:1008918929036.

42. Pawlik, A.; Rehman, M.A.U.; Nawaz, Q.; Bastan, F.E.; Sulka, G.D.; Boccaccini, A.R. Fabrication and Characterization of Electrophoretically Deposited Chitosan-Hydroxyapatite Composite Coatings on Anodic Titanium Dioxide Layers. *Electrochim. Acta* **2019**, *307*, 465–473, doi:https://doi.org/10.1016/j.electacta.2019.03.195.

Preprints (www.preprints.org) | NOT PEER-REVIEWED | Posted: 27 June 2022 doi:10.20944/preprints202206.0352.v1

43. Hum, J.; Naseri, S.; Boccaccini, A.R. Bioactive Glass Combined with Zein as Composite Material for the Application in Bone Tissue Engineering. *Biomed. Glas.* **2018**, *4*, 72–81, doi:doi:10.1515/bglass-2018-0007.

44. ASTM D3359-17, ASTM International, West Conshohocken, PA, 2017 Standard Test Methods for Rating Adhesion by Tape Test.

45. ASTM D4541-17, ASTM International, West Conshohocken, PA, 2017 Standard Test Method for Pull-Off Strength of Coatings Using Portable Adhesion Testers.

46. 4624:2016, I.; Adhesion Paints and Varnishes — Pull-off Test for Adhesion.

47. ASTM D3363-20, ASTM International, West Conshohocken, PA, 2020 Standard Test Method for Film Hardness by Pencil Test.

48. ASTM B571-97(2008)e1, ASTM International, West Conshohocken, PA, 2008 Standard Practice for Qualitative Adhesion Testing of Metallic Coatings.

49. Kokubo, T.; Takadama, H. How Useful Is SBF in Predicting in Vivo Bone Bioactivity? *Biomaterials* **2006**, *27*, 2907–2915, doi:10.1016/j.biomaterials.2006.01.017.

50. Aqib, R.; Kiani, S.; Bano, S.; Wadood, A.; Ur Rehman, M.A. Ag–Sr Doped Mesoporous Bioactive Glass Nanoparticles Loaded Chitosan/Gelatin Coating for Orthopedic Implants. *Int. J. Appl. Ceram. Technol.* **2021**, *18*, 544–562, doi:10.1111/ijac.13702.

51. Neščáková, Z.; Zheng, K.; Liverani, L.; Nawaz, Q.; Galusková, D.; Kaňková, H.; Michálek, M.; Galusek, D.; Boccaccini, A.R. Multifunctional Zinc Ion Doped Sol – Gel Derived Mesoporous Bioactive Glass Nanoparticles for Biomedical Applications. *Bioact. Mater.* **2019**, *4*, 312–321, doi:10.1016/j.bioactmat.2019.10.002.

52. Besra, L.; Liu, M. A Review on Fundamentals and Applications of Electrophoretic Deposition (EPD). *Prog. Mater. Sci.* **2007**, *52*, 1–61, doi:10.1016/j.pmatsci.2006.07.001.

53. Choudhary, R.; Khurana, D.; Kumar, A.; Subudhi, S. Stability Analysis of Al2O3/Water Nanofluids. *J. Exp. Nanosci.* **2017**, *12*, 140–151, doi:10.1080/17458080.2017.1285445.

54. Bouman, J.; Belton, P.; Venema, P.; Van Der Linden, E.; De Vries, R.; Qi, S. Controlled Release from Zein Matrices: Interplay of Drug Hydrophobicity and PH. *Pharm. Res.* **2016**, *33*, 673–685, doi:10.1007/s11095-015-1818-8.

55. Pishbin, F.; Simchi, A.; Ryan, M.P.; Boccaccini, A.R. Electrophoretic Deposition of Chitosan/45S5 Bioglass® Composite Coatings for Orthopaedic Applications. *Surf. Coatings Technol.* **2011**, *205*, 5260–5268, doi:https://doi.org/10.1016/j.surfcoat.2011.05.026.

56. Sikkema, R.; Baker, K.; Zhitomirsky, I. Electrophoretic Deposition of Polymers and Proteins for Biomedical Applications.

Preprints (www.preprints.org) | NOT PEER-REVIEWED | Posted: 27 June 2022 doi:10.20944/preprints202206.0352.v1

Adv. Colloid Interface Sci. **2020**, *284*, 102272, doi:10.1016/j.cis.2020.102272.

57. Meyer, N.; Rivera, L.R.; Ellis, T.; Qi, J.; Ryan, M.P.; Boccaccini, A.R. Bioactive and Antibacterial Coatings Based on Zein/Bioactive Glass Composites by Electrophoretic Deposition. *Coatings* 2018, *8*.

58. Sarkar, P.; Nicholson, P.S. Electrophoretic Deposition (EPD): Mechanisms, Kinetics, and Application to Ceramics. *J. Am. Ceram. Soc.* 1996, *79*, 1987–2002.

59. Aguilar-Rabiela, A.E.; Leal-Egaña, A.; Nawaz, Q.; Boccaccini, A.R. Integration of Mesoporous Bioactive Glass Nanoparticles and Curcumin into PHBV Microspheres as Biocompatible Composite for Drug Delivery Applications. *Molecules* **2021**, *26*, doi:10.3390/molecules26113177.

60. Westhauser, F.; Wilkesmann, S.; Nawaz, Q.; Hohenbild, F.; Rehder, F.; Saur, M.; Fellenberg, J.; Moghaddam, A.; Ali, M.S.; Peukert, W.; et al. Effect of Manganese, Zinc, and Copper on the Biological and Osteogenic Properties of Mesoporous Bioactive Glass Nanoparticles. *J. Biomed. Mater. Res. - Part A* **2021**, *109*, 1457–1467, doi:10.1002/jbm.a.37136.

61. Westhauser, F.; Wilkesmann, S.; Nawaz, Q.; Schmitz, S.I.; Moghaddam, A.; Boccaccini, A.R. Osteogenic Properties of Manganese-Doped Mesoporous Bioactive Glass Nanoparticles. *J. Biomed. Mater. Res. A* **2020**, *108*, 1806–1815, doi:10.1002/jbm.a.36945.

62. Ahmed, Y.; Nawaz, A.; Singh Virk, R.; Wadood, A.; Ur Rehman, M.A. Fabrication and Characterization of Zein/Bioactive Glass Deposited on Pretreated Magnesium via Electrophoretic Deposition. *Int. J. Ceram. Eng. Sci.* **2020**, *2*, 254–263, doi:https://doi.org/10.1002/ces2.10066.

63. Shaikh, S.; Khatri, Z.; Oh, K.W.; Kim, I.-S.; Kim, S. Zein/Cellulose Acetate Hybrid Nanofibers: Electrospinning and Characterization. *Macromol. Res.* **2014**, *22*, 971–977, doi:10.1007/s13233-014-2136-4.

64. Ureña, J.; Tsipas, S.; Jiménez-Morales, A.; Gordo, E.; Detsch, R.; Boccaccini, A.R. Cellular Behaviour of Bone Marrow Stromal Cells on Modified Ti-Nb Surfaces. *Mater. Des.* **2018**, *140*, 452–459, doi:10.1016/j.matdes.2017.12.006.

65. Ur Rehman, M.A.; Bastan, F.E.; Nawaz, A.; Nawaz, Q.; Wadood, A.; Rehman, M.A.U.; Bastan, F.E.; Nawaz, A.; Nawaz, Q.; Wadood, A. Electrophoretic Deposition of PEEK/Bioactive Glass Composite Coatings on Stainless Steel for Orthopedic Applications: An Optimization for in Vitro Bioactivity and Adhesion Strength. *Int. J. Adv. Manuf. Technol.* **2020**, *108*, 1849–1862, doi:10.1007/s00170-020-05456-x.

66. Mariotti, C.E.; Ramos-Rivera, L.; Conti, B.; Boccaccini, A.R. Zein-Based Electrospun Fibers Containing Bioactive Glass with Antibacterial Capabilities. *Macromol. Biosci.* **2020**, *20*, doi:10.1002/mabi.202000059.

67. Sadasivuni, K.K.; Saha, P.; Adhikari, J.; Deshmukh, K.; Ahamed, M.B.; Cabibihan, J.-J. Recent Advances in Mechanical Properties of Biopolymer Composites: A Review. *Polym. Compos.* **2020**, *41*, 32–59, doi:https://doi.org/10.1002/pc.25356.

Preprints (www.preprints.org) | NOT PEER-REVIEWED | Posted: 27 June 2022 doi:10.20944/preprints202206.0352.v1